Chapter 9

# MEASURING INTERFACIAL ROUGHNESS BY POLARIZED OPTICAL SCATTERING

Thomas A. Germer

*Optical Technology Division*
*National Institute of Standards and Technology*
*Gaithersburg, MD 20899*

germer@nist.gov

**Abstract**    Polarized optical scatter measurements yield information that can be used to identify sources of scatter. In this chapter, we review measurements of angle-resolved polarized optical scattering and their application to the measurement of roughness of surfaces and thin films.

**Keywords:** bidirectional reflectance distribution function; rough surfaces; polarization; interfacial roughness; thin films

## 1.    Introduction

Optical scattering measurements are extremely sensitive for locating and characterizing defects, contamination, and roughness on smooth surfaces. Its sensitive, high-throughput, and non-destructive nature has made optical scattering the preferred method for inspecting many materials whose surfaces must be pristine before manufacturing devices on them, such as polished silicon for the semiconductor microelectronics industry, substrates for magnetic storage media, and glass used for information display systems.[1] Optical scattering often limits the performance of optics, such as those used for satellite telescopes or ring-laser gyroscopes. Understanding and being able to measure roughness can aid manufacturers in developing these materials. Lastly, the morphology of thin films is determined by the mechanisms of film growth and the interactions between the interfaces, and measurements of the relative

roughness and correlation between the interfaces can yield significant information about the underlying physics in these systems.[2]

Since there may be a number of different sources of optical scatter in a material or thin film besides roughness, such as material inhomogeneity, subsurface defects, or particles, it may be important to distinguish among the different sources in order to properly interpret optical scattering measurements. Recent research has demonstrated that the polarization of light scattering can be instrumental in this application.[3–7] Theoretical and experimental results have shown that different scattering sources yield unique polarization signatures that can be used to distinguish scattering sources or validate the interpretation of intensity data.

This chapter will discuss the measurement and interpretation of roughness by angle-resolved optical scattering with an emphasis on utilizing information contained in the polarization. In Sec. 2, we will describe how to quantify scattered light in terms of its intensity and polarization properties. In Sec. 3, we will discuss measurement methods. In Sec. 4, we will describe roughness of a single interface, where we use the polarization information primarily to validate the interpretation. In Sec. 5, we will describe the scattering by the two layers of a dielectric film and show how the polarization can yield information about the relative amplitude and correlation between the roughness of the two interfaces. In the final section, Sec. 6, we will make some remarks about extending the technique to more interfaces.

## 2.   Definitions

Angle-resolved measurements are concerned with quantifying light originating from a source direction, defined by a polar angle $\theta_i$ and azimuthal angle $\phi_i$, and scattered into a reflected direction, defined by a polar angle $\theta_r$ and azimuthal angle $\phi_r$. One quantity describing the directional dependence of scatter from a surface is the bidirectional reflectance distribution function (BRDF), defined historically[8] as the differential radiance $dL_r$ (power per unit solid angle per unit projected surface area) scattered by a uniformly illuminated, homogeneous material per unit differential incident irradiance $dE_i$ (power per unit surface area):

$$f_r(\theta_i, \phi_i, \theta_r, \phi_r) = \frac{dL_r(\theta_i, \phi_i, \theta_r, \phi_r)}{dE_i(\theta_i, \phi_i)} \tag{9.1}$$

Eq. (9.1), while often quoted, is of little practical use, because most materials are not homogeneous and most illumination schemes are not uniform. That is, even if a material does not have appreciable variation across its surface, any real specimen has a finite extent. Likewise, while

we can generate illumination that is approximately uniform within some region, that region of illumination must come to an end, if not simply at the specimen edge. The biggest problem with this definition is that diffuse materials often emit light outside of a finitely illuminated region. When we see Eq. (9.1), but ignore the words surrounding it, then we can easily find ourselves coping with an apparently infinite BRDF in certain regions of the sample.

An equivalent definition of the BRDF considers the average power $\langle \Phi_r \rangle$ scattered into a solid angle $\Omega$ for a given incident power $\Phi_i$:

$$f_r(\theta_i, \phi_i, \theta_r, \phi_r) = \lim_{\Omega \to 0} \frac{\langle \Phi_r \rangle}{\Phi_i \Omega \cos \theta_r} \tag{9.2}$$

That is, the BRDF is the average fraction of light scattered per *projected* solid angle for a finitely illuminated region. It is a distribution in the scattering direction and a function of incident direction. It is also a function of wavelength, polarization, and sample properties.

While the BRDF appears to have a term (i.e., $\cos \theta_r$) that might cause it to diverge for large scattering angles, most surface scattering sources behave in such a manner that the scattering per unit solid angle falls off in angle fast enough that the BRDF not only remains finite, but approaches zero for $\theta_r \to 90°$. In real data, however, this may not be true. Rayleigh scatter by air within the field of view of the receiver, a primary background source in smooth surface scatter measurements, and other sources of stray light do not vanish at large scattering angles.[9] Furthermore, small uncertainties in the scattering angle can lead to apparent uncertainties in the BRDF, which do not translate to meaningful uncertainties for some applications. A convenient property of the BRDF is that it obeys Helmholtz reciprocity:

$$f_r(\theta_i, \phi_i, \theta_r, \phi_r) = f_r(\theta_r, \phi_r, \theta_i, \phi_i) \tag{9.3}$$

The definition of the BRDF given in Eq. (9.2) does not fully characterize the scatter properties of a material, though, because it fails to include any details of how scatter depends upon incident polarization or what polarization the scattered light is. The addition of information contained in the polarization makes measurements of the polarization attractive.

To characterize polarization states, the Mueller-Stokes formalism is convenient.[10] Any intensity-like quantity (e.g., power, radiance, irradi-

ance, etc.) can be quantified in terms of a Stokes vector, given by

$$\mathbf{\Phi} = \begin{pmatrix} \Phi_{\mathrm{s}} + \Phi_{\mathrm{p}} \\ \Phi_{\mathrm{s}} - \Phi_{\mathrm{p}} \\ \Phi_{\mathrm{s+p}} - \Phi_{\mathrm{s-p}} \\ \Phi_{\mathrm{lcp}} - \Phi_{\mathrm{rcp}} \end{pmatrix} \tag{9.4}$$

where $\Phi_u$ is the power that we would measure if we used an analyzer that passes only $u$-polarized light: s indicating that the electric field is perpendicular to the plane defined by the direction of propagation and the surface normal, p indicating that the electric field is parallel to that plane, s±p indicating that the electric field is ±45° with respect to those directions, and lcp and rcp indicating left- and right-circularly polarized light, respectively. We can describe how a material interacts with light, assuming that the material's effect upon the light is linear, using a $4 \times 4$ Mueller matrix, which relates an input Stokes vector to an output Stokes vector. A Mueller matrix BRDF, $\mathbf{F}_{\mathrm{r}}$, can then be defined as the Mueller matrix that relates the average scattered Stokes vector power $\langle \mathbf{\Phi}_{\mathrm{r}} \rangle$ to the incident Stokes vector power $\mathbf{\Phi}_{\mathrm{i}}$:[11]

$$\lim_{\Omega \to 0} \frac{\langle \mathbf{\Phi}_{\mathrm{r}} \rangle}{\Omega} = \mathbf{F}_{\mathrm{r}} \mathbf{\Phi}_{\mathrm{i}} \cos \theta_{\mathrm{r}} \tag{9.5}$$

Note that we have rearranged Eq. (9.5), compared to Eq. (9.2), since one cannot divide a Stokes vector by another Stokes vector. Furthermore, we cannot measure $\mathbf{F}_{\mathrm{r}}$ with a single measurement.

In many applications, measurement of the full Mueller matrix BRDF is not necessary to yield the information we need. Rather, a specific incident polarization, which may depend upon incident and scattered directions, is chosen to maximize differentiation among scattering mechanisms, and we measure the Stokes vector of the scattered light. Sometimes, instead of reporting the Stokes vector elements, a different combination of them is reported. One set of parameters consists of the BRDF for the given incident polarization, $f_{\mathrm{r}}$, the principal angle of the polarization ellipse, $\eta$, the degree of circular polarization, $P_C$, and the total degree of polarization $P$. These parameters are related to the measured Stokes vector intensity by

$$f_{\mathrm{r}} = \langle \Phi_{\mathrm{r0}} \rangle / (\Omega \ \Phi_{\mathrm{i}} \cos \theta_{\mathrm{r}})$$

$$\eta = \tan^{-1}(\langle \Phi_{\mathrm{r2}} \rangle / \langle \Phi_{\mathrm{r1}} \rangle)$$

$$P_{\mathrm{C}} = \langle \Phi_{\mathrm{r3}} \rangle / \langle \Phi_{\mathrm{r0}} \rangle \tag{9.6}$$

$$P = \sqrt{\langle \Phi_{\mathrm{r1}}^2 \rangle + \langle \Phi_{\mathrm{r2}}^2 \rangle + \langle \Phi_{\mathrm{r3}}^2 \rangle} / \langle \Phi_{\mathrm{r0}} \rangle$$
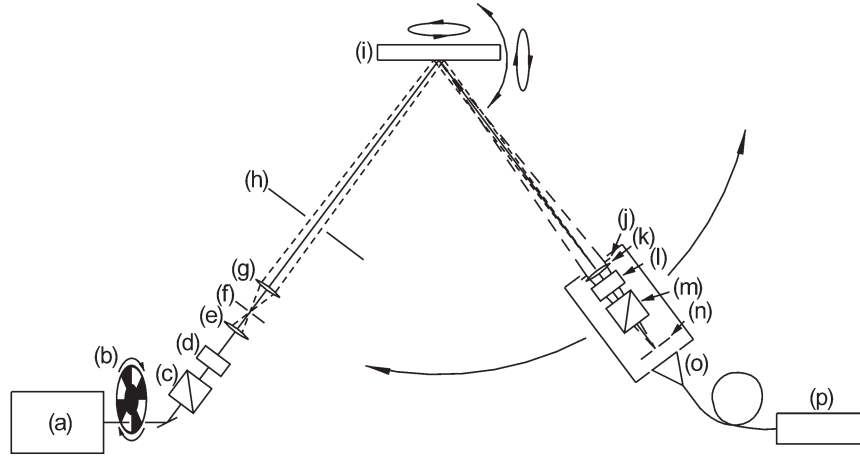
*Figure 9.1.* A schematic diagram of a polarization-resolved, angle-resolved scatterometer: (a) laser, (b) chopper, (c) source polarizer, (d) source rotating retarder, (e) spatial filter lens, (f) spatial filter, (g) primary lens or mirror, (h) baffling, (i) sample, (j) receiver aperture, (k) receiver lens, (l) receiver rotating retarder, (m) receiver polarizer, (n) field stop, (o) detector, and (p) lock-in amplifier.

where $\Phi_{rj}$ $(j = 0, 1, 2, 3)$ is the $j$-th element of $\mathbf{\Phi}_r$. One reason these parameters are particularly useful is that all of the information about the intensity is contained in one parameter $(f_r)$, and all of the information about the randomness of the polarization is contained in another parameter $(P)$. In many cases, the parameter $\eta$ is all that is necessary to differentiate scattering mechanisms, since $P_C$ is often predicted to be negligible.

While Stokes vector analysis has been used to distinguish and quantify different scattering sources, at least for well chosen measurement conditions, Mueller matrix analysis has not yet been found to yield additional information on isotropic surfaces that warrants the added difficulty that the measurements entail. However, it is not inconceivable that Mueller matrix analysis will find itself useful for patterned or other anisotropic samples.

## 3.    Measurement Methods

Figure 9.1 shows a schematic diagram of an instrument used for performing angle-resolved optical scatter measurements.[12] While there are a variety of guides that exist for developing BRDF instruments,[1,13,14] we will summarize a number of their most important features. We can

divide these instruments into three parts: the source [elements (a)–(h) in Fig. 9.1], the sample holder and goniometer [element (i) in Fig. 9.1], and the receiver [elements (j)–(p) in Fig. 9.1]. Details of the design of each of these parts depends upon our application. In this discussion, we will concentrate on those issues which are important for polarimetric measurements of nanoscale roughness.

The purpose of the source is to generate the beam of polarized incident light. The source consists of a laser (a), which is modulated by an optical chopper (b). The polarization state of the incident light is set by a fixed plane polarizer (c) and a rotatable linear retarder (d). Elements (a)–(d), plus the various mirrors that are needed to steer the beam around the table, generally impart some stray light on the beam. In order that the beam incident upon the sample have as good a beam profile as possible, the beam is spatially filtered with a lens and pinhole [(e) and (f)]. Finally, a focusing element (g) focuses the beam onto the entrance aperture of the receiver (j). The focusing element can be a lens or a concave mirror. In order to have the least amount of stray light at small scattering angles, a high-quality concave mirror is usually preferred for this element. Finally, some baffling (h) or enclosure is usually included. The baffling should not actually block any of the beam, since that will generally scatter strongly and increase the stray light in the system.

The sample holder and goniometer is designed to orient the sample (i) with respect to the source. A simple system may employ a single rotation axis, enabling scatter measurements in the plane of incidence. A more complex system with more axes of rotation enables measurements out of the plane of incidence and as functions of sample rotation. Lastly, linear translation of the sample may be needed to assess sample uniformity by obtaining scatter measurements from multiple spots on a sample.

The purpose of the receiver is to collect and analyze light over a known solid angle about a given direction. The receiver rotates about the illumination spot on the sample. The first element of the receiver is the receiver aperture (j). The area $A$ of this aperture and its distance $R$ from the sample determines the collected solid angle $\Omega = A/R^2$. A lens (k) in the receiver images the sample onto a field stop (n), so that the size of the field stop aperture determines the sample field of view. A smaller field of view reduces the amount of stray light accepted by the receiver. It should be set so that it is as small as possible, but always so that the field of view is larger than the illuminated area on the sample. The combination of a rotating retarder (l) and a fixed polarizer (m) selects a specific polarization state for analysis. A detector (o) is placed

after the field stop, and a lock-in amplifier (p), synchronized with the chopper, is used for phase sensitive detection of the signal.

The dynamic range of angle-resolved light scattering instrumentation presents a challenge to accurate measurements of nanoscale roughness. Near the specular direction, the intensity can be very high, and the BRDF measurement is limited by the diffraction-limited spot size of the incident light on the receiver aperture. For a Gaussian beam focused onto the detector, the maximum measurable BRDF at normal incidence is[1]

$$f_r^{\text{max}} = \frac{\pi D^2}{2\lambda^2} \tag{9.7}$$

where $D$ is the diameter of the illumination spot at the sample and $\lambda$ is the wavelength of the light. For $D = 5$ mm and $\lambda = 550$ nm, the maximum value of the BRDF is about $10^8$ sr$^{-1}$. In the other extreme, the measured scatter signal is limited by Rayleigh scatter by air surrounding the sample. That is, the field of view of the receiver will accept scatter from the beam propagating through the air. In the absence of a sample, this quantity is given approximately by[9]

$$f_r^{\text{Rayleigh}} = \frac{4\pi^2(n-1)^2 l_{\text{FOV}}}{\lambda^4 N \sin\theta \cos\theta_r} \times \left\{ \begin{array}{ll} 1 & \text{for s-polarization} \\ \cos^2\theta & \text{for p-polarization} \end{array} \right. \tag{9.8}$$

where $\theta$ is the viewing angle measured from the incident direction, $l_{\text{FOV}}$ is the diameter of the field of view of the receiver, $N$ is the number density of air, and $n$ is the index of refraction of air. At 20 °C, standard atmospheric pressure, $\lambda = 550$ nm, viewing perpendicular to the beam propagation direction, s-polarized incident light, and for $l_{\text{FOV}} = 10$ mm, Eq. (9.8) yields a BRDF of approximately $1.5 \times 10^{-8}$ sr$^{-1}$. With the reasonable assumption that we need to have signals above this level (although it is conceivable that one could subtract this scatter from data), the range of scatter levels extends a range of over 16 orders of magnitude.

The wide dynamic range can be obtained by a combination of multiple collection apertures and multiple detectors. The smallest aperture should be on the order of the beam diameter $2w_0$ at the detector,

$$2w_0 = \frac{2\lambda R}{\pi D} \tag{9.9}$$

For $R = 500$ mm and $D = 5$ mm, the beam diameter is about 70 $\mu$m in diameter. As one varies the direction away from the specular direction, larger apertures need to be used, the largest typically spanning an angle from 0.5° to 2°. One cannot use just two apertures, however, for a number of reasons. First, the ratio of areas in these extremes is at least
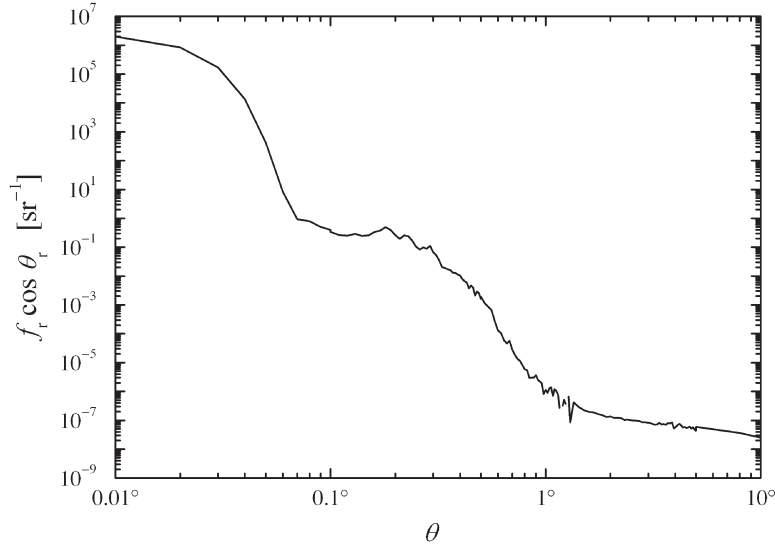
*Figure 9.2.* An instrument signature measured for an angle-resolved instrument at the author's institute.

5000, increasing the dynamic range requirements of the detector. More importantly, a well-designed instrument will have sufficiently low stray light that at an angle where use of the small aperture encounters signals at the noise floor of the detector, opening up to the largest detector may actually accept the full specular beam to the detector. Therefore, any instrument should have a range of apertures, each varying by a factor of 4 to 7 from the next.

In addition to using multiple receiver apertures, multiple detectors can significantly expand the dynamic range of a scattering instrument. The detectors should have overlapping ranges of use, and the least sensitive detector should be capable of measuring the incident power. It is common to employ a silicon photodiode and a photomultiplier tube, for example, as the two detectors.

Figure 9.2 shows a representative measurement of an instrument signature, measured by scanning the receiver through the incident beam in the absence of a sample. Three regimes can be observed: the coherent incident beam at small angles ($\theta < 0.06°$), stray light at intermediate angles ($0.06° < \theta < 1°$), and Rayleigh scatter at large angles ($\theta > 1°$). The challenge of the instrument designer (and to some extent, the user, who must maintain the instrument) is to create an optical system that transitions to the Rayleigh scatter regime in as small an angle as possible. Low scatter optics, well-placed baffling, and reduction of the field

of view of the detector to its minimum necessary size serve to reduce the stray light. The effect of an aperture change can be seen in Fig. 9.2 near $\theta = 1°$, where the noise level appears to rise before the next aperture can be used.

We must also consider the effect of laser speckle. For a spatially-incoherent source of diameter $D$ at the sample, the coherence length at the receiver aperture will be approximately given by the same expression as Eq. (9.9), within a small factor which depends upon the intensity profile over the source. If one considers a source of diameter $D$, an aperture of diameter $D_{\text{det}}$, and a source-aperture distance $R$, there will be approximately

$$N_{\text{speckle}} = \frac{\pi D_{\text{det}}^2/4}{\pi w_0^2} = \left(\frac{\pi D D_{\text{det}}}{2\lambda R}\right)^2 \qquad (9.10)$$

speckles entering the receiver.[15] Assuming Poisson statistics, the relative standard deviation of the signals will be given by

$$\frac{\sigma_S}{\langle S \rangle} = \frac{1}{\sqrt{N_{\text{speckle}}}} = \frac{2\lambda R}{\pi D D_{\text{det}}} = \frac{\lambda}{D\sqrt{\pi\Omega}} \qquad (9.11)$$

For a $D = 5$ mm source, a $D_{\text{det}} = 5$ mm aperture, $R = 500$ mm, and $\lambda = 550$ nm, the estimated relative standard deviation would be 0.7 %. While this is an acceptable value for many measurements, reduction of the illumination spot diameter or the detector aperture can easily place this value into a regime where laser speckle is by far the largest source of measurement uncertainty.

There are a number of ways to overcome speckle noise, of which some applications may be able to take advantage. The easiest in many applications is simply to make several measurements, either at different locations on the sample or at different sample rotations. Constant motion of the sample during the measurement can also effectively allow sampling over different surface realizations. Destroying the spatial coherence of the light source can be performed by a number of methods, including passing the beam through an ultrasonically-vibrated multi-mode fiber. Such a beam, however, will necessarily have poorer focusing characteristics, and the angular resolution of the system will be degraded.

To perform measurements of the Mueller matrix BRDF, we must analyze the scattered polarization for a number of incident polarizations. A common method for obtaining the Mueller matrix is the $\omega$-$5\omega$ scheme, developed by Azzam,[16] whereby a quarter-wave retarder on the source [(d) in Fig. 9.1] is rotated at frequency $\omega$, while another quarter-wave retarder on the receiver [(l) in Fig. 9.1] is rotated at frequency $5\omega$. The

Mueller matrix elements are then linearly related to the Fourier components of the signal. An improvement on this scheme uses $0.37\lambda$ retarders instead of $0.25\lambda$ retarders, in order to improve the path on the Poincarré sphere taken by each of the rotating retarders.[17,18] Other methods employ the use of liquid crystal variable retarders[19] and photoelastic modulators.[20] Many measurements do not require full measurement of the Mueller matrix. For example, in most of the measurements presented in this chapter, only a single linearly polarized source is used, and the Stokes vector of the scattered light is measured. In that case, a rotating half-wave retarder can be used in the source to rotate the polarization into the desired angle.

## 4.    Roughness of a Single Interface

## 4.1    Theory

We will begin our discussion of measurements with roughness of the interface between a condensed state (usually a solid, but could be a liquid) and a gas or vacuum. This case is the usual starting point for measurements of nanoscale roughness. If we assume that the surface height function $\Delta z(\boldsymbol{\rho})$ $[\boldsymbol{\rho} = (x, y)]$ is single valued, has zero mean, is much smaller than the wavelength of the light, and that the slopes $\partial \Delta z(\boldsymbol{\rho})/\partial x$ and $\partial \Delta z(\boldsymbol{\rho})/\partial z$ are much smaller than one, the problem can be solved by first-order perturbation theory. The solution was first proposed by Rice in 1951,[21] while a more complete solution was developed by Barrick in 1970.[22] The Mueller matrix BRDF from a rough surface in the smooth surface approximation is given by

$$\mathbf{F}_{\mathrm{r}} = \frac{16\pi^2}{\lambda^4} \cos\theta_{\mathrm{i}} \cos\theta_{\mathrm{r}} \langle |Z(\boldsymbol{\kappa})|^2 \rangle \, \mathbf{Q} \qquad (9.12)$$

where the Mueller matrix $\mathbf{Q} = \mathbf{M}(\mathbf{q}, \mathbf{q}^\dagger)$ is non-depolarizing, and the function $\mathbf{M}$ is given in the Appendix. The scattering matrix $\mathbf{q}$ has elements

$$
\begin{aligned}
q_{\mathrm{ss}} &= (\epsilon - 1)k^2 \cos\phi_{\mathrm{r}}/[(k_{z\mathrm{i}} + k'_{z\mathrm{i}})(k_{z\mathrm{r}} + k'_{z\mathrm{r}})] \\
q_{\mathrm{ps}} &= -(\epsilon - 1)k k'_{z\mathrm{r}} \sin\phi_{\mathrm{r}}/[(k_{z\mathrm{i}} + k'_{z\mathrm{i}})(\epsilon k_{z\mathrm{r}} + k'_{z\mathrm{r}})] \\
q_{\mathrm{sp}} &= -(\epsilon - 1)k k'_{z\mathrm{i}} \sin\phi_{\mathrm{r}}/[(\epsilon k_{z\mathrm{i}} + k'_{z\mathrm{i}})(k_{z\mathrm{r}} + k'_{z\mathrm{r}})] \\
q_{\mathrm{pp}} &= (\epsilon - 1)(\epsilon k_{xy\mathrm{i}} k_{xy\mathrm{r}} - k'_{z\mathrm{i}} k'_{z\mathrm{r}} \cos\phi_{\mathrm{r}})/[(\epsilon k_{z\mathrm{i}} + k'_{z\mathrm{i}})(\epsilon k_{z\mathrm{r}} + k'_{z\mathrm{r}})]
\end{aligned}
\qquad (9.13)
$$

where

$$
\begin{aligned}
k'_{z\beta} &= k(\epsilon - \sin^2\theta_\beta)^{1/2} \\
k_{z\beta} &= k\cos\theta_\beta \\
k_{xy\beta} &= k\sin\theta_\beta \\
k &= 2\pi/\lambda
\end{aligned}
\tag{9.14}
$$

$(\beta = \mathrm{i}, \mathrm{r})$. $\langle |Z(\boldsymbol{\kappa})|^2 \rangle$ is the two-dimensional power spectral density (PSD) of the surface height function, where

$$
Z(\boldsymbol{\kappa}) = \lim_{A\to\infty} \frac{1}{\sqrt{A}} \int_A \mathrm{d}^2\boldsymbol{\rho}\, \Delta z(\boldsymbol{\rho}) \exp(\mathrm{i}\,\boldsymbol{\kappa}\cdot\boldsymbol{\rho})
\tag{9.15}
$$

The surface wavevector $\boldsymbol{\kappa}$ has elements $\kappa_x$ and $\kappa_y$ given by the diffraction equations,

$$
\begin{aligned}
\kappa_x &= k_{xy\mathrm{r}}\cos\phi_\mathrm{r} - k_{xy\mathrm{i}} \\
\kappa_y &= k_{xy\mathrm{r}}\sin\phi_\mathrm{r}
\end{aligned}
\tag{9.16}
$$

In the above, we are ignoring, without loss of generality, the azimuthal angle of the source direction, $\phi_\mathrm{i}$. That is, we are defining our $x$-axis to be the intersection of the plane of incidence and the plane of the sample. The specular condition is $\theta_\mathrm{i} = \theta_\mathrm{r}$ and $\phi_\mathrm{r} = 0$. The surface wavevector (radians per unit length) is related to the spatial frequency (cycles per unit length) by a factor of $2\pi$, so PSDs are often presented with respect to $|\boldsymbol{\kappa}|/(2\pi)$.

The limit in Eq. (9.15) does not exist for a randomly rough surface of infinite extent. It is precisely that issue that gives rise to the observed speckle pattern. In practice, however, a non-zero solid angle is collected. The limit of $|Z(\boldsymbol{\kappa})|^2$ integrated over a finite region of spatial frequencies does, in fact, exist. Notice that the Mueller matrix $\mathbf{Q}$ does not depend upon $Z(\boldsymbol{\kappa})$. So, while there will exist a speckle pattern in the intensity, that speckle pattern does not exist in the polarization.

The expressions in Eqs. (9.13) appear to be very similar to Fresnel reflection coefficients. In fact, $|q_{ss}|^2$ is given by

$$
|q_\mathrm{ss}|^2 = [R_\mathrm{s}(\theta_\mathrm{i}) R_\mathrm{s}(\theta_\mathrm{r})]^{1/2}
\tag{9.17}
$$

where $R_\mathrm{s}(\theta)$ is the specular reflectance of the substrate for s-polarization and incident angle $\theta$. Thus, in the absence of specific values of the dielectric constant $\epsilon$, it is relatively straightforward to make measurements that can be used to obtain $|q_\mathrm{ss}|^2$.

## 4.2    Limitations

An estimate of the maximum roughness amplitude that can be treated with the first-order approach can be found by considering diffraction from a sinusoidal grating.[23] Within the Kirchhoff approximation, the ratio of the second-order diffraction efficiency to the first-order diffraction efficiency is given by

$$[J_2(\delta)/J_1(\delta)]^2 \approx \delta^2 \qquad (9.18)$$

where $\delta = ka(\cos\theta_i + \cos\theta_r)$ and $a$ is the amplitude of the sinusoid. If we ask the question, "When is the second-order diffraction intensity less than 5 % of the first-order diffraction intensity?" we find a characteristic amplitude $a$. Since the rms roughness is given by $\sigma = a/\sqrt{2}$, we arrive at a practical estimate of the validity of the first-order theory:

$$\sigma < \frac{\lambda}{10(\cos\theta_i + \cos\theta_r)} \qquad (9.19)$$

The expression shows that the perturbative approach can be valid for relatively large roughnesses, as long as the incident and scattering angles are large. This behavior can be easily observed by noticing that nearly all materials become specularly reflecting when viewed at grazing incidence. The measurement scheme where $\theta_i$ and $\theta_r$ are held equal and fixed at large angles, while $\phi_r$ is varied provides a means for measuring the roughness of surfaces approaching the wavelength of the light.[24]

## 4.3    The Inverse Problem

The proportionality between the BRDF and the surface PSD, given in Eq. (9.12), makes optical scattering an attractive method for measuring surface roughness in the smooth surface limit. One need only solve Eq. (9.12) for $\langle|Z(\boldsymbol{\kappa})|^2\rangle$, taking into account the incident polarization. For example, for s-polarized light, and performing measurements in the plane of incidence, we can use Eq. (9.17) to obtain the relatively simple expression

$$\langle|Z(\boldsymbol{\kappa})|^2\rangle = \frac{\lambda^4\langle\Phi_r\rangle}{16\pi^2\Omega\Phi_i\cos\theta_i\cos\theta_r^2[R_s(\theta_i)R_s(\theta_r)]^{1/2}} \qquad (9.20)$$

The range of surface wavevectors $|\boldsymbol{\kappa}|$ over which the measurement can be performed is limited at small $|\boldsymbol{\kappa}|$ by the range of angles over which the signal is sufficiently above the instrument signature and at large $|\boldsymbol{\kappa}|$ by the wavelength of the light. For example, if the minimum angle from the specular direction is $0.1°$, and we are operating with $\lambda = 550$ nm and an

incident angle of $\theta_i = 60°$, the smallest spatial frequency is $|\kappa|_{min}/(2\pi) \approx$ 1.5 mm$^{-1}$, and the largest spatial frequency is $|\kappa|_{max}/(2\pi) \approx 3$ $\mu$m$^{-1}$, a range spanning almost three orders of magnitude.

While roughness can contribute to elastic light scattering, many other sources can also contribute and interfere with the results. For example, Rayleigh scatter in the air, particles on the surface, subsurface defects, material inhomogeneities, and stray light can contribute to varying degrees. Therefore, if we want to apply Eq. (9.12) to data to determine the roughness statistics, it is important that we test the basic hypothesis that roughness is indeed causing the scatter. There are a number of measurements we can make to check that the scatter is consistent with roughness.

The first of these consistency checks is angle scaling. That is, we can perform a scattering measurement using one incident angle, use Eq. (9.12) to estimate the PSD, then try the same measurement using a different incident angle. The problem with this method is that it can be quite deceptive. Scatter by material inhomogeneities, for example, has been shown to yield very similar results as roughness.[6, 25, 26] Just as the scattering by roughness is proportional to the PSD of the surface height function, the scattering by inhomogeneities is proportional to the PSD of the dielectric constant across the surface. Since the dependence upon direction in both cases depends upon those PSDs evaluated using the same diffraction equation, what we end up showing more than anything else is that the diffraction equation works.

A second consistency check that is often used is wavelength scaling.[1] Here, we perform the measurement at multiple wavelengths and, again, compare the estimated PSDs determined from Eq. (9.12). Subsurface defects and material inhomogeneities have scattering behaviors that are very similar, especially if the dielectric constant of the material does not change appreciably. For this reason, this method is often employed using very wide ranges of wavelengths, over which the dielectric constant of the material varies significantly. Over such a wide range of wavelengths, the measurement becomes substantially more difficult to perform, because we need to switch optical components and detectors. It also fails to tell us whether any of the scatter results from roughness, just that it does not result from roughness over the entire wavelength range. Despite these problems, it has been considered the mainstay for checking for roughness scatter, and was instrumental in helping recognize that many mirror materials, such as beryllium and aluminum, were inherently high scatterers, regardless of how smooth they were, because they tend to exhibit a high degree of scatter from material inhomogeneity.[27]

14

The third consistency check, polarization analysis, is much more powerful and relatively difficult to fool.[7] With this method, we are checking for consistency with the elements of the scattering matrix, Eq. (9.13). Scattering by other sources, such as particles, subsurface defects, and material inhomogeneity, yield scattering matrix elements that differ from those given in Eqs. (9.13).[6,7] For example, the scattering matrix elements appropriate for subsurface defects or material inhomogeneity are given by[6,25,26] $q_{ss}^{sub} = q_{ss}$, $q_{sp}^{sub} = q_{sp}$, $q_{ps}^{sub} = q_{ps}$, and

$$q_{pp}^{sub} = (\epsilon - 1)(k_{xyi}k_{xyr} - k'_{zi}k'_{zr}\cos\phi_r)/[(\epsilon k_{zi} + k'_{zi})(\epsilon k_{zr} + k'_{zr})] \quad (9.21)$$

That is, only the pp-terms differ, and even then, only when $\theta_i$ and $\theta_r$ are both non-zero. Purely s-polarized incident light, for example, will yield no discrimination between these two scattering mechanisms. Thus, we must have some p-polarized light incident on the sample and use large incident and scattering polar angles. These restrictions argue for measurements out of the plane of incidence. For example, a useful measurement, which maps out the PSD over a wide range of surface wavevectors, is to set $\theta_i = \theta_r$ and vary $\phi_r$ from $0°$ to $180°$. The incident polarization is linear at an angle $\eta_i$ and continuously varied from $45°$ to $135°$ over this range, such that when $\phi_r = 90°$, the incident light is p-polarized ($\eta_i = 90°$). That is,

$$\eta_i = 45° + \phi_r/2 \quad (9.22)$$

The magnitude of the surface wavevector is then given by

$$|\boldsymbol{\kappa}| = 2k \sin\theta_r \sin(\phi_r/2) \quad (9.23)$$

At each angle, the Stokes vector can be measured. In many instances, we only need to measure the linear components of the Stokes vector, because we expect little circular polarization from surface roughness, if the material is non- or weakly- absorbing.

We can obtain reasonably good discrimination between scattering sources by performing the measurement in the plane of incidence by measuring the Stokes vector for $45°$ incident polarization. However, near the surface normal, that discrimination disappears, and we are left confirming the roughness hypothesis at the beginning and end of a scan, and hoping that at those angles near the surface normal the trend continues.

We can also perform Mueller matrix measurements to distinguish scattering sources. However, since s-polarized incident light has very little ability to discriminate sources, we would not expected that Mueller measurements would improve our confidence of the roughness hypothesis substantially from what we can obtain by optimizing the incident polarization to that which gives the largest discrimination.

It is interesting to note that, because the scatter by roughness in the smooth surface limit yields a deterministic polarization, the light scattered by such a rough surface does not depolarize the light.[28] While we observe speckle fluctuations in the intensity, especially if we use a small collection solid angle, little of those fluctuations are observed in the polarization state. Thus, polarization measurements often appear quite noise-free in comparison to their intensity counterparts.

## 4.4 Example

To demonstrate the methodology described in Sec. 4.3, we present data obtained from a thick metallic TiN layer grown on a silicon wafer. The thickness of the layer, 110 nm, is thick enough and the material absorbent enough that we can safely ignore any interfaces below the TiN. The light scattering measurement was carried out using $\lambda = 532$ nm light with $\theta_i = \theta_r = 60°$, varying the scattering azimuthal angle $\phi_r$ from near 0° to 170°. The polarization was varied as described in Eq. (9.22). The results of the measurements are shown in Fig. 9.3, in terms of the parameters given in Eqs. (9.6). The systematic uncertainties in the measurement are less than the size of the symbols, and the random uncertainties can be estimated by observing the variation of the data about a smooth curve.

We evaluated the polarization predicted by first-order vector perturbation theory. We chose $\epsilon = 1.6 + 4.6i$ so that the results matched in the specular direction, which is equivalent to using specular ellipsometry to determine its value. The measured polarization states agree very well with the predictions of the perturbation theory, which are shown as solid curves in Fig. 9.3. In particular, the measured $P$ is close to one, within about 15 %, the deviations of which may be due to stray light in the experiment. The parameters $P_C$ and $\eta$ follow very closely to the curves.

Another likely scattering mechanism in metallic samples is scattering by material inhomogeneity. We show $\eta$ and $P_C$ predicted by Eq. (9.21) for this mechanism in Fig. 9.3, too. The data do not agree with such scattering. Scatter by particles, which depends upon particle size, yield different behaviors, as well.[6, 29, 30] It is clear from the comparison that the data agree very well with the microroughness theory and that the differentiation among the alternate scattering mechanisms is unambiguous. Thus, the polarization measurement establishes the validity of the microroughness interpretation, allowing us to convert the measured BRDF to the PSD of the surface height function.

The result of converting the BRDF to PSD is shown in Fig. 9.4. The results show fractal behavior for large $\boldsymbol{\kappa}$, where $\langle |Z(\boldsymbol{\kappa})|^2 \rangle \propto |\boldsymbol{\kappa}|^{-2.8}$, and
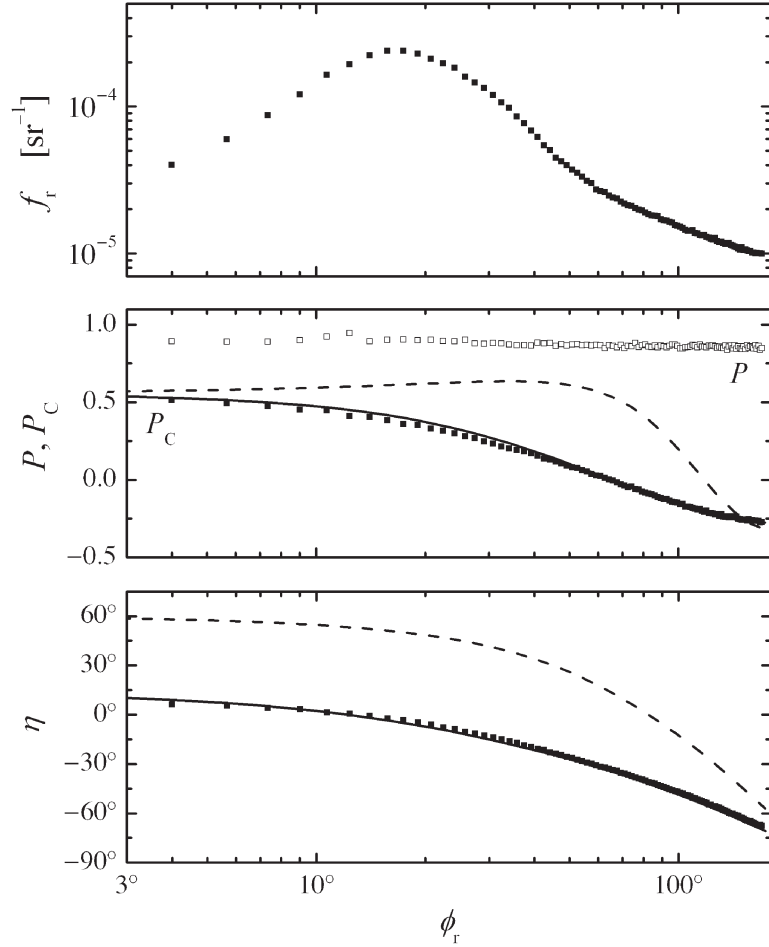
*Figure 9.3.* Results from out-of-plane ($\theta_i = \theta_r = 60°$) polarized light scattering measurements (symbols) for a TiN sample using 532 nm light: (top) the BRDF, $f_r$, (middle) the degrees of polarization and circular polarization, (open symbols) $P$ and (closed symbols) $P_C$, respectively, and (bottom) the principal polarization angle $\eta$. The incident polarization was varied as described in Eq. (9.22) in the text. The curves represent the polarization states predicted for light scattered by (solid) a microrough surface and (dashed) material inhomogeneity.
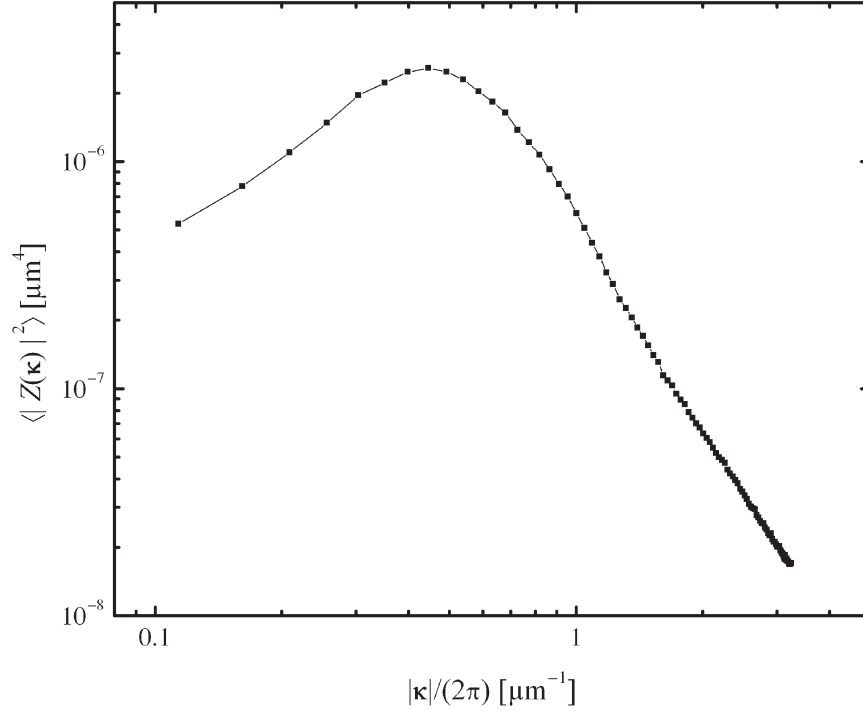
*Figure 9.4.*   The PSD of the surface height function derived from the data shown in Fig. 9.3.

a distinct peak in the power spectrum near $|\boldsymbol{\kappa}|/(2\pi) = 0.45 \ \mu\text{m}^{-1}$. By integrating the two-dimensional PSD, we can obtain an estimate of the rms roughness. The total rms roughness over the bandwidth shown is about 2.6 nm.

The excellent agreement between the theory and experiment for microroughness implies that the polarization of light scattered by microroughness is not determined by the exact details of the surface height profile, but is a unique signature of the scattering mechanism. It therefore suggests that scatterometers can be designed to be blind to microroughness. For example, a device may be constructed with a number of detectors, each viewing a particular scattering direction, and each with a polarizer aligned to block the light from microroughness.[31] Such a device would collect light over a large solid angle, be microroughness-blind, and therefore be more sensitive to other sources of scatter, such as subsurface defects and particulate contamination.

## 5.  Roughness of Two Interfaces

In Sec. 4, we described measurements that only used the polarization to validate the interpretation of the intensity. In this section, we will describe measurements in which the polarization is not used to validate the model, but is used to extract information about interface roughness. In this case, we are interested in the two interfaces of a dielectric film. The methodology that we describe parallels that used by specular ellipsometry[10, 32] to determine film thickness. By performing an ellipsometric measurement of light diffusely scattered out of the specular direction, we move away from $\kappa = 0$ and probe the *variations* in film thickness. That is, we measure the relative interface roughness and its degree of correlation.[33, 34]

## 5.1  Theory

We now consider a film, having dielectric constant $\epsilon_f$ and mean thickness $\tau$ lying above a substrate of dielectric constant $\epsilon$. The surface height functions of the buried and exposed interfaces are $\Delta z_1$ and $\Delta z_2$, respectively (leaving out the explicit dependence on $\boldsymbol{\rho}$). We apply first-order vector perturbation theory to this problem. The zero-order, unperturbed ($\Delta z_1 = 0$ and $\Delta z_2 = 0$) fields are found from the solution of the well-known problem of reflection from a dielectric film. The first-order calculation consists of expanding the electric and magnetic fields on both sides of each interface and the local surface normal to first order in the surface height functions $\Delta z_j$ about their mean. The requirement that the tangential electric and magnetic fields be continuous across the boundary leads to relationships between zero-order and first-order fields. The theory self-consistently handles the multiple reflections that occur for both orders of the field. However, since it assumes that the film thickness is constant, it does not account for long-range non-conformal roughness, which has sufficient amplitude to substantially vary the local film thickness. In order for the theory to be valid, the modulations of the surface height functions, $\Delta z_j$, must be much less than the wavelength, $\lambda$, and the surface slope must be small.

Elson[35–39] described the solution to the first-order vector perturbation theory for scattering from interfacial microroughness in a dielectric stack. For the buried interface (1), the scattering matrix $\mathbf{q}^{(1)}$ to replace $\mathbf{q}$ in Eq. (9.12) has elements

$$q_{uv}^{(1)} = 4(\epsilon - \epsilon_f)k_{zi}''k_{zr}'' \exp[\mathrm{i}(k_{zi}'' + k_{zi}'' - k_{zr} - k_{zr})\tau]s_{uv}^{(1)} \qquad (9.24)$$

$(u,\ v = \mathrm{s},\ \mathrm{p})$ where

$$s_{\mathrm{ss}}^{(1)} = -k^2 \cos\phi_{\mathrm{r}}/(\Gamma_{\mathrm{si}}\Gamma_{\mathrm{sr}})$$

$$s_{\mathrm{ps}}^{(1)} = \epsilon_{\mathrm{f}} k k_{z\mathrm{i}}' \sin\phi_{\mathrm{r}}/(\Gamma_{\mathrm{pi}}\Gamma_{\mathrm{sr}})$$

$$s_{\mathrm{sp}}^{(1)} = \epsilon_{\mathrm{f}} k k_{z\mathrm{r}}' \sin\phi_{\mathrm{r}}/(\Gamma_{\mathrm{si}}\Gamma_{\mathrm{pr}})$$

$$s_{\mathrm{pp}}^{(1)} = -\epsilon_{\mathrm{f}}(\epsilon k_{xy\mathrm{i}}k_{xy\mathrm{r}} - \epsilon_{\mathrm{f}}k_{z\mathrm{i}}k_{z\mathrm{r}}\cos\phi_{\mathrm{r}})/(\Gamma_{\mathrm{pi}}\Gamma_{\mathrm{pr}})$$

$$\tag{9.25}$$

$$\Gamma_{\mathrm{p}\beta} = \epsilon_{\mathrm{f}} F_{\mathrm{p}\beta}^{(+)} k_{z\beta} - F_{\mathrm{p}\beta}^{(-)} k_{z\beta}''$$

$$\Gamma_{\mathrm{s}\beta} = F_{\mathrm{s}\beta}^{(+)} k_{z\beta} - F_{\mathrm{s}\beta}^{(-)} k_{z\beta}''$$

$$\tag{9.26}$$

$$F_{\mathrm{p}\beta}^{(\pm)} = \epsilon_{\mathrm{f}} K_{\beta}^{(\mp)} k_{\beta}' - \epsilon K_{\beta}^{(\pm)} k_{z\beta}''$$

$$F_{\mathrm{s}\beta}^{(\pm)} = K_{\beta}^{(\mp)} k_{z\beta}' - K_{\beta}^{(\pm)} k_{z\beta}''$$

$$K_{\beta}^{(\pm)} = \exp(2\mathrm{i}k_{z\beta}''\tau) \pm 1$$

$$\tag{9.27}$$

$k_{z\beta}'' = k(\epsilon_{\mathrm{f}} - \sin^2\theta_\beta)^{1/2}$ ($\beta = \mathrm{i}$ or $\mathrm{r}$). The Fourier transform of the roughness of the $m$-th interface is given above in Eq. (9.15), with $\Delta z$ replaced with $\Delta z_m$. For the exposed interface (2), the scattering matrix $\mathbf{q}^{(2)}$ to replace $\mathbf{q}$ in Eq. (9.12) has elements

$$q_{uv}^{(2)} = (\epsilon_{\mathrm{f}} - 1)\exp[-\mathrm{i}(k_{z\mathrm{i}} + k_{z\mathrm{r}})\tau]s_{uv}^{(2)} \tag{9.28}$$

where

$$s_{\mathrm{ss}}^{(2)} = -k^2 F_{\mathrm{si}}^{(+)} F_{\mathrm{sr}}^{(+)} \cos\phi_{\mathrm{r}}/(\Gamma_{\mathrm{si}}\Gamma_{\mathrm{sr}})$$

$$s_{\mathrm{ps}}^{(2)} = -k k_{z\mathrm{i}}'' F_{\mathrm{pi}}^{(-)} F_{\mathrm{sr}}^{(+)} \sin\phi_{\mathrm{r}}/(\Gamma_{\mathrm{pi}}\Gamma_{\mathrm{sr}})$$

$$s_{\mathrm{sp}}^{(2)} = -k k_{z\mathrm{r}}'' F_{\mathrm{si}}^{(+)} F_{\mathrm{pr}}^{(-)} \sin\phi_{\mathrm{r}}/(\Gamma_{\mathrm{si}}\Gamma_{\mathrm{pr}})$$

$$s_{\mathrm{pp}}^{(2)} = -(\epsilon_{\mathrm{f}} k_{xy\mathrm{i}}k_{xy\mathrm{r}} F_{\mathrm{pi}}^{(+)} F_{\mathrm{pr}}^{(+)} - k_{z\mathrm{i}}'' k_{z\mathrm{r}}'' F_{\mathrm{pi}}^{(-)} F_{\mathrm{pr}}^{(-)} \cos\phi_{\mathrm{r}})/(\Gamma_{\mathrm{pi}}\Gamma_{\mathrm{pr}})$$

$$\tag{9.29}$$

Just as the matrix elements for scattering by single-interface roughness given in Eq. (9.13) are independent of the surface height function, those for scattering by the two interfaces of a dielectric film given in Eqs. (9.25) and (9.29) do not depend upon the respective surface height functions. Therefore, to first order, the scattering from a single rough interface will not depolarized light. Furthermore, the fields resulting from the scattering of each interface are independent of each other.

We can evaluate the special case of two interfaces that are totally conformal (correlated and equal roughness) by coherently adding the scattering matrices from each of them:

$$\mathbf{q}^{(\text{corr})} = \mathbf{q}^{(1)} + \mathbf{q}^{(2)} \tag{9.30}$$

Similarly, if the two interfaces are equally rough, but have a random phase relationship between them (i.e., they are uncorrelated), then we can add the two sources incoherently:

$$\mathbf{Q}^{(\text{uncorr})} = \mathbf{M}(\mathbf{q}^{(1)}, \mathbf{q}^{(1)\dagger}) + \mathbf{M}(\mathbf{q}^{(2)}, \mathbf{q}^{(2)\dagger}) \tag{9.31}$$

In general, the surfaces may be neither correlated nor of equal roughness. In this case, we replace the factor $\mathbf{Q}\langle|Z|^2\rangle$ in Eq. (9.12) by

$$\langle|Z|^2\rangle\mathbf{Q} = \langle\mathbf{M}(Z_1\mathbf{q}^{(1)} + Z_2\mathbf{q}^{(2)}, Z_1^*\mathbf{q}^{(1)\dagger} + Z_2^*\mathbf{q}^{(2)\dagger})\rangle \tag{9.32}$$

where we have dropped the explicit dependence of $Z_m$ on $\boldsymbol{\kappa}$. Since the only random variables are $Z_1$ and $Z_2$, Eq. (9.32) can be simplified to

$$
\begin{aligned}
\langle|Z|^2\rangle\mathbf{Q} = \quad &\langle|Z_1|^2\rangle\mathbf{M}(\mathbf{q}^{(1)}, \mathbf{q}^{(1)\dagger}) + \langle|Z_2|^2\rangle\mathbf{M}(\mathbf{q}^{(2)}, \mathbf{q}^{(2)\dagger}) \\
&+ 2\mathrm{Re}\langle Z_1 Z_2^*\rangle\mathrm{Re}\mathbf{M}(\mathbf{q}^{(1)}, \mathbf{q}^{(2)\dagger}) \\
&- 2\mathrm{Im}\langle Z_1 Z_2^*\rangle\mathrm{Im}\mathbf{M}(\mathbf{q}^{(1)}, \mathbf{q}^{(2)\dagger})
\end{aligned} \tag{9.33}
$$

## 5.2    The Inverse Problem

Eq. (9.33) is an overdetermined equation in the PSD of the two interfaces, $\langle|Z_1|^2\rangle$ and $\langle|Z_2|^2\rangle$, and the cross-PSD, $\langle Z_1 Z_2^*\rangle$. That is, we can write Eq. (9.33) in the form $\langle|Z|^2\rangle\mathbf{Q} = \mathbf{DZ}$, where $\mathbf{D}$ is a $16 \times 4$ matrix

$$\mathbf{D} = \begin{pmatrix} \mathbf{M}(\mathbf{q}^{(1)}, \mathbf{q}^{(1)\dagger}) \\ \mathbf{M}(\mathbf{q}^{(2)}, \mathbf{q}^{(2)\dagger}) \\ 2\mathrm{Re}\mathbf{M}(\mathbf{q}^{(1)}, \mathbf{q}^{(2)\dagger}) \\ -2\mathrm{Im}\mathbf{M}(\mathbf{q}^{(1)}, \mathbf{q}^{(2)\dagger}) \end{pmatrix} \tag{9.34}$$

where each row consists of a flattened $4 \times 4$ matrix, and $\mathbf{Z}$ is a four element column vector,

$$\mathbf{Z} = \begin{pmatrix} \left\langle|Z_1|^2\right\rangle \\ \left\langle|Z_2|^2\right\rangle \\ \mathrm{Re}\left\langle Z_1 Z_2^*\right\rangle \\ \mathrm{Im}\left\langle Z_1 Z_2^*\right\rangle \end{pmatrix} \tag{9.35}$$

We can solve for $\mathbf{Z}$ in a least-squares sense by calculating the pseudoinverse, $\mathbf{D}^{-1} = (\mathbf{D}^{\mathrm{T}}\mathbf{D})^{-1}\mathbf{D}^{\mathrm{T}}$. Thus, we can determine the roughness

statistics for the two interfaces of a thin film from the measured Mueller matrix BRDF $\mathbf{F}_r$ from Eqs. (9.12),

$$\mathbf{Z} = \frac{\lambda^4}{16\pi^2 \cos\theta_i \cos\theta_r}(\mathbf{D}^T\mathbf{D})^{-1}\mathbf{D}^T\mathbf{F}_r \qquad (9.36)$$

Let us consider the simpler case of a specific incident polarization state, specified by a unit intensity Stokes vector $\mathbf{S}$. The scattered Stokes vector will then be given by left-multiplying $\mathbf{S}$ by Eq. (9.33):

$$\begin{aligned}
\langle|Z|^2\rangle\mathbf{QS} = \quad & \langle|Z_1|^2\rangle\mathbf{M}(\mathbf{q}^{(1)},\mathbf{q}^{(1)\dagger})\mathbf{S} \\
& +\langle|Z_2|^2\rangle\mathbf{M}(\mathbf{q}^{(2)},\mathbf{q}^{(2)\dagger})\mathbf{S} \\
& +2\mathrm{Re}\langle Z_1 Z_2^*\rangle\mathrm{Re}\mathbf{M}(\mathbf{q}^{(1)},\mathbf{q}^{(2)\dagger})\mathbf{S} \\
& -2\mathrm{Im}\langle Z_2 Z_1^*\rangle\mathrm{Im}\mathbf{M}(\mathbf{q}^{(2)},\mathbf{q}^{(1)\dagger})\mathbf{S}
\end{aligned} \qquad (9.37)$$

Eq. (9.37) is a fully determined equation in the roughness statistics. That is, Eq. (9.37) can be written as $\langle|Z|^2\rangle\mathbf{QS} = \mathbf{D}'\mathbf{Z}$, where $\mathbf{D}'$ is a $4 \times 4$ matrix

$$\mathbf{D}' = \begin{pmatrix} \mathbf{M}(\mathbf{q}^{(1)},\mathbf{q}^{(1)\dagger})\mathbf{S} \\ \mathbf{M}(\mathbf{q}^{(2)},\mathbf{q}^{(2)\dagger})\mathbf{S} \\ 2\mathrm{Re}\mathbf{M}(\mathbf{q}^{(1)},\mathbf{q}^{(2)\dagger})\mathbf{S} \\ -2\mathrm{Im}\mathbf{M}(\mathbf{q}^{(1)},\mathbf{q}^{(2)\dagger})\mathbf{S} \end{pmatrix} \qquad (9.38)$$

and each row is the transpose of a 4 element vector. Eq. (9.38) can be inverted, provided the two surfaces scatter with different polarization states. Thus, the four degrees of freedom of a measured Stokes BRDF $\mathbf{f}_r$ map onto the four degrees of freedom of the roughness statistics:

$$\mathbf{Z} = \frac{\lambda^4}{16\pi^2 \cos\theta_i \cos\theta_r}(\mathbf{D}')^{-1}\mathbf{f}_r \qquad (9.39)$$

It is convenient for us to define a relative roughness

$$\chi = \sqrt{\langle|Z_1|^2\rangle/\langle|Z_2|^2\rangle} \qquad (9.40)$$

and a complex correlation coefficient

$$c = \langle Z_1 Z_2^*\rangle/\sqrt{\langle|Z_1|^2\rangle\langle|Z_2|^2\rangle} \qquad (9.41)$$

Just as there is one constraint on a Stokes vector $(S_0^2 \geq S_1^2 + S_2^2 + S_3^2)$, the parameter $c$ must satisfy $|c| \leq 1$. For most realistic surfaces, $c$ should have no imaginary component. It is interesting to note that the intensity and the polarization state of the scattered light separate in much the same way as for single interface roughness: the polarization state uniquely determines $\chi$ and $c$, while the intensity, once $\chi$ and $c$ are known,
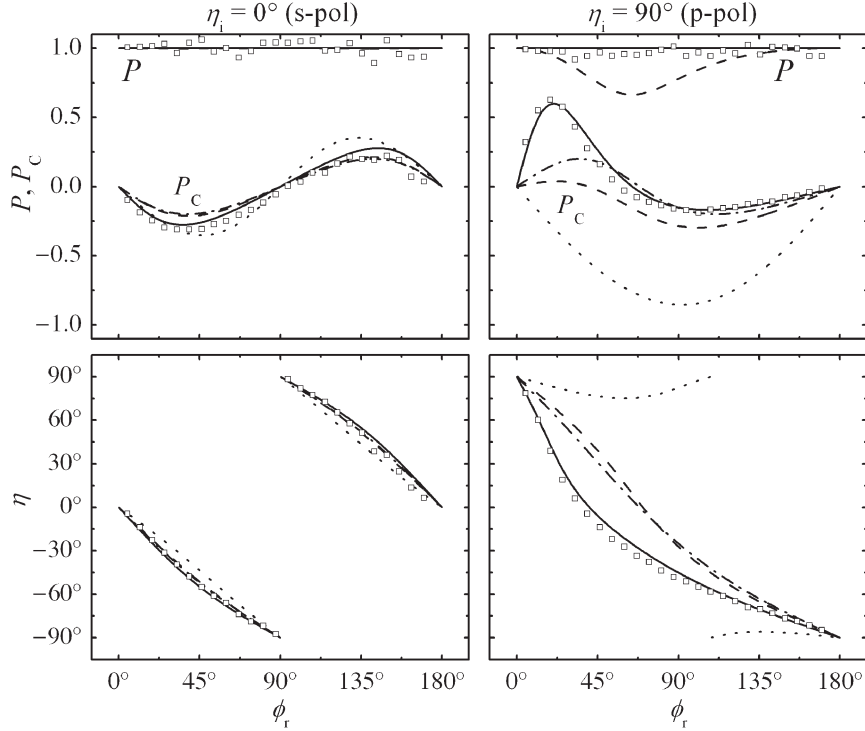
*Figure 9.5.* Polarization parameters $P$, $P_{\mathrm{C}}$, and $\eta$ for scattering out of the plane of incidence from (solid) correlated and equal roughness, (dashed) uncorrelated and equal roughness, (dotted) roughness of the exposed interface, (dash-dot) roughness of the buried interface, and (symbols) experimental results from a $SiO_2$ layer grown on microrough silicon. The incident light was (left column) s-polarized and (right column) p-polarized. Other parameters in the model are described in the text.

determines the magnitude of the PSDs of the two interfaces. Another point to note is that when $|c| = 1$, we will observe no depolarization. In this case, there is no randomness in the ratio or relative phase of both sources, and so there is no randomness in their sum. Depolarization only occurs when there is incoherence between two sources.

## 5.3    Example

To demonstrate the application of the perturbation theory analysis for roughness of a dielectric film, we consider the behavior of $\lambda = 632.8$ nm light scattered by a 52 nm $SiO_2$ ($\epsilon_{\mathrm{f}} = 2.13$) layer grown on a silicon ($\epsilon = 15.07 + 0.15i$) substrate. We let the incident angle be $\theta_{\mathrm{i}} = 60°$ and scattering angle be $\theta_{\mathrm{r}} = 60°$.

Before we present experimental results, we will make a number of observations about the theoretical predictions for four different limiting cases of interfacial roughness (roughness of each interface alone, correlated, and uncorrelated roughness). Figure 9.5 shows the scattered polarization state as a function of $\phi_r$ for s- and p-polarized incident light calculated for these cases. The results for s-polarized incident light (left column of Fig. 9.5) show only a small amount of differentiation between the roughness conditions, with none existing at $\phi_r = 0°$, $90°$, and $180°$. These results are similar to what we found for a single interface in Sec. 4 above. Symmetry dictates the polarization for $\phi_r = 0°$, $90°$, and $180°$: for s-polarized light incident upon an isotropic sample in the static approximation, the scattered field must be anti-symmetric about the incident plane and symmetric about the perpendicular plane. Therefore, in the plane of incidence ($\phi_r = 0°$ and $180°$), the scattered light must be s-polarized ($s_{sp} = s_{ps} = 0$) , while for $\phi_r = 90°$, the scattered light must be p-polarized ($s_{ss} = 0$).

The results for p-polarized incident light (right column of Fig. 9.5) show significantly greater differentiation between the different limiting cases, as long as we are sufficiently out of the plane of incidence (i.e., $\phi_r \neq 0°$ or $180°$). Again, symmetry requires that the scattered light be p-polarized in the plane of incidence. However, symmetry no longer exists about the perpendicular plane, so that for $\phi_r = 90°$, each case can yield a different polarization. Previous measurements have exploited this geometry to differentiate scattering from small particles, single rough surfaces, and subsurface defects.[7] We are often interested in extracting roughness statistics from data over as wide range of surface wavevectors as possible. Since there is little differentiation between cases near $\phi_r = 0°$, the dynamic range of available spatial frequencies is limited.

Fig. 9.6 presents two schemes that differentiate between interfacial roughness conditions for most scattering angles. One of these schemes uses circularly polarized incident light (left column of Fig. 9.6). Another scheme changes the incident polarization state as the viewing direction is varied. In the right column of Fig. 9.6, the incident light is linearly polarized, varied according to Eq. (9.22), as was done above for the single interface roughness measurements. We observe reasonably good differentiation between the different roughness conditions at most scattering angles, using either of the two schemes, with somewhat better differentiation observed for the varying incident polarization scheme.

Because measurements out of the plane of incidence generally require more complicated instrumentation than those required for measurements in the plane of incidence, we include two schemes that work reasonably well in the plane of incidence. Figure 9.7 shows calculated polariza-
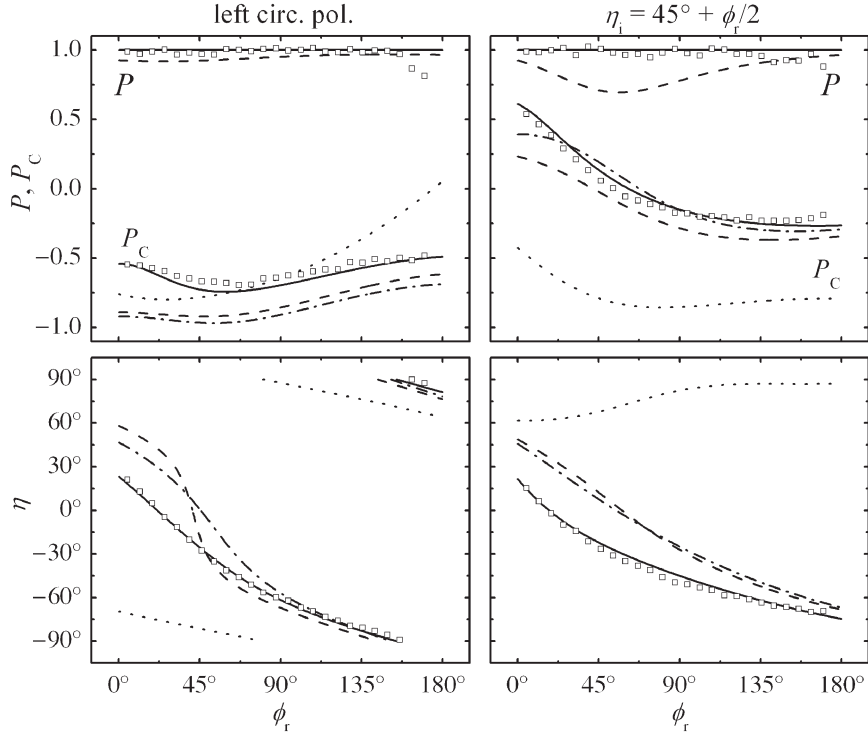
*Figure 9.6.* Polarization parameters $P$, $P_C$, and $\eta$ for scattering out of the plane of incidence from (solid) correlated and equal roughness, (dashed) uncorrelated and equal roughness, (dotted) roughness of the exposed interface, (dash-dot) roughness of the buried interface, and (symbols) experimental results from a $SiO_2$ layer grown on microrough silicon. The incident light was (left column) left circularly polarized and (right column) linearly polarized at an angle $\eta_i = 45° + \phi_r/2$. Other parameters in the model are described in the text.

tion parameters for the different roughness conditions evaluated in the plane of incidence ($\theta_i = 60°$, $\phi_r = 0°$). Since the scattering matrices are diagonal for this geometry, we do not show results for s-polarized or p-polarized incident light. Incident light of either circular polarization or 45° linear polarization maps the four independent Mueller matrix elements onto the four Stokes vector elements. While we observe discrimination between the roughness cases in Fig. 9.7, it is relatively weak, with numerous curves crossing near $\theta_r = 0°$.

The results for polarized light scattering measurements from a 52 nm $SiO_2$ film thermally grown on a photolithographically-produced microrough silicon surface are included in Figs. 9.5–9.7. The microrough surface consisted of a pseudorandom distribution of nominally 8 nm deep
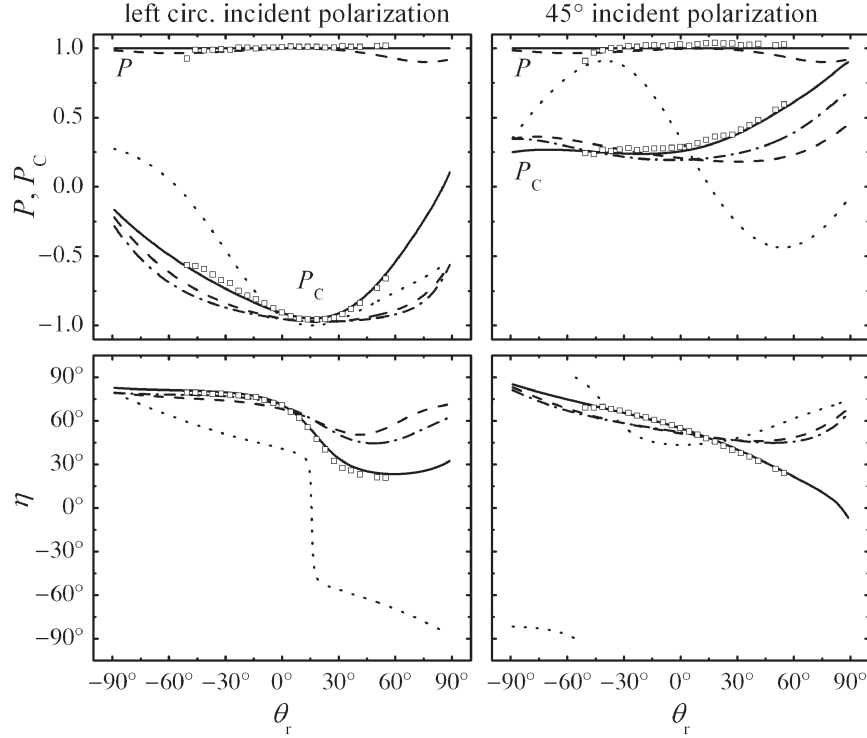
*Figure 9.7.* Polarization parameters $P_C$, $P$, and $\eta$ for scattering in the plane of incidence from (solid) correlated and equal roughness, (dashed) uncorrelated and equal roughness, (dotted) roughness of the exposed interface, (dash-dot) roughness of the buried interface, and (symbols) experimental results from a $SiO_2$ layer grown on microrough silicon. The incident light was (left column) left circularly polarized and (right column) linearly polarized at an angle $\eta_i = 45°$. Other parameters in the model are described in the text.

circular pits having diameters of nominally 1.31 $\mu$m and 1.76 $\mu$m.[40] Details of the experiment, its uncertainties, and the sample are given elsewhere.[12,33] This system should exhibit conformal roughness, at least for small surface wavevectors. The results shown in Figs. 9.5–9.7 indeed behave most like the equal roughness model for all incident polarizations, though close inspection of the results reveals small discrepancies, which result from the buried interface being smoother than the exposed interface. The relative roughness of the two interfaces ($\chi$) and the correlation coefficient $c$ can be extracted using the technique outlined in Sec. 5.2. Figure 9.8 shows $c$ and $\chi$ as functions of spatial frequency extracted from the data shown in Figs. 9.5–9.7. The indicated uncertainties represent single standard deviations of the extracted results obtained from the

26
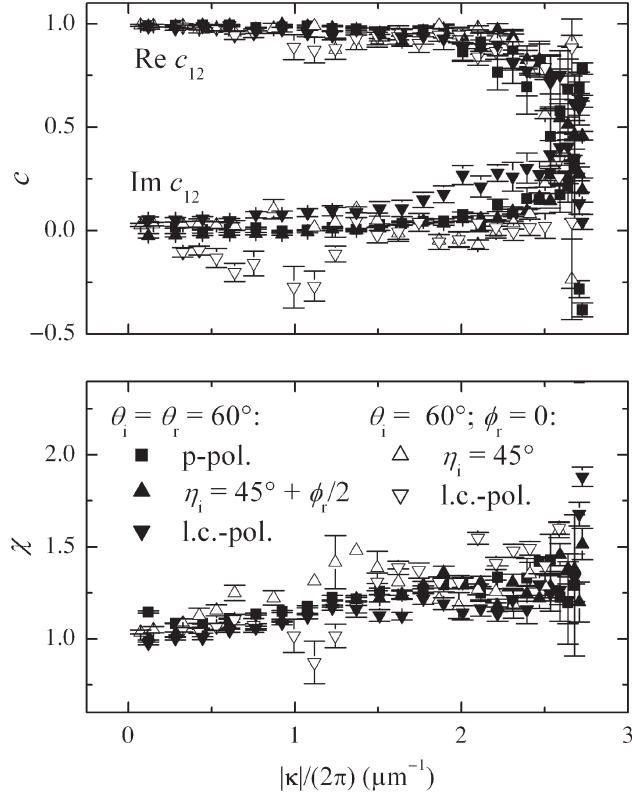


*Figure 9.8.* Roughness parameters extracted from polarized light scattering measurements from the 52 nm SiO$_2$ layer thermally grown on silicon. The results are obtained from measurements out of the plane of incidence (solid symbols) and in the plane of incidence (open symbols).

statistical uncertainties in the original data. The results obtained from all incident polarizations are consistent with each other, showing $\chi > 1$ and $c \approx 1$ for most spatial frequencies. Further validation of the method has been achieved by performing the measurements at multiple wavelengths and incident angles.[33] While measurements of the full Mueller matrix may allow different scattering mechanisms to be distinguished and quantified using the analysis given in Sec. 5.2, the results shown in Fig. 9.5 suggest that certain incident polarization states do not allow for much differentiation.

Figure 9.8 includes the results using data obtained in the plane of incidence. Large uncertainties and discrepancies result from the poor discrimination near 1 $\mu$m$^{-1}$. Comparison between the results of Figs. 9.5–9.7 suggest that maximum discrimination between different roughness

conditions occurs in directions out of the plane of incidence. Other calculations show that such improvements also tend to occur for other scattering sources such as particles or subsurface defects.[6] While other researchers have performed light scattering ellipsometry measurements in the plane of incidence,[41] we chose to make full use of the polarization by performing such measurements in out-of-plane geometries.

It is noteworthy to point out that in Figs. 9.5–9.7, the theoretical predictions for buried interface roughness and uncorrelated roughness are the most poorly resolved. In both cases, the roughness of the bottom interface is present, and the top interface is incoherent with the bottom interface. When sources are incoherent, they add as intensities, rather than as fields, so that the smaller field has a correspondingly smaller effect. Hence, when the dielectric contrast between the substrate and the film is much larger than between film and the ambient environment, which is the case for our example, uncorrelated roughness of the top interface will be more difficult to observe in the presence of buried interface roughness.

In many realistic cases, any correlations between two interfaces are expected to be such that $c$ is real and lies in the interval $0 \leq c \leq 1$. Any imaginary component to $c$ implies a lateral offset in the roughness function. For this reason, it may be reasonable to use Eq. (9.39) to obtain a starting point for the roughness statistics, but to constrain Im $c = 0$ and perform a least-squares fit of the theory to the data.

We have also investigated a number of other systems, including a case of anti-correlated roughness (nominal $c = -1$) and a case of offset roughness [nominal $c = \exp(i\boldsymbol{\kappa} \cdot \mathbf{R})$, where $\mathbf{R}$ is a lateral offset in the two roughness functions].[42, 43] These cases were much more complicated to analyze. While the amplitude of the roughness was small compared to the wavelength of the light, the lack of correlation caused unacceptably large variations in the thickness throughout the film. Thus, we find that the analysis presented here has much more rigid requirements in terms of the tolerable roughness amplitude over which the theory is valid.

## 6.    Final Comments

It is worth considering, at the end, whether it is worth extending this methodology to three or more interfaces (that is, two or more films). After all, the space of valid Mueller matrices can be shown to be spanned by four scattering matrices. For example, we can decompose any valid Mueller matrix $\mathbf{M}$ into the sum

$$\mathbf{M} = \sum_{j=0}^{3} \sum_{k=0}^{3} a_{jk} \mathbf{M}(\boldsymbol{\sigma}_j, \boldsymbol{\sigma}_k^\dagger) \qquad (9.42)$$

where $\boldsymbol{\sigma}_j$ are the Pauli matrices given in the Appendix, and the 16 coefficients obey $a_{jk} = a_{kj}^*$. Therefore, one ought to be able to extract the roughness statistics for up to four interfaces from a Mueller matrix scattering measurement. However, the method would be very limited. In the specular direction, the scattering matrix for any interface will not have any off-diagonal elements, so only two of the four basis matrices are available. Since we cannot differentiate the different interfaces near the specular direction, the technique would therefore have a very narrow range of spatial frequencies over which to operate.

## Appendix: $4 \times 4$ Matrix Product of Two Scattering Matrices

We define a $4 \times 4$ matrix product $\mathbf{M}(\mathbf{q}_1, \mathbf{q}_2)$ between two $2 \times 2$ scattering matrices, such that its elements are given by

$$\mathbf{M}(\mathbf{q}_1, \mathbf{q}_2)_{jk} = \frac{1}{2}\mathrm{Tr}\left(\mathbf{q}_1 \boldsymbol{\sigma}_k \mathbf{q}_2 \boldsymbol{\sigma}_j\right) \tag{9.A.1}$$

$(j, k = 0, 1, 2, 3)$ where the Pauli matrices are

$$\boldsymbol{\sigma}_0 = \begin{pmatrix} 1 & 0 \\ 0 & 1 \end{pmatrix} \quad \boldsymbol{\sigma}_1 = \begin{pmatrix} 1 & 0 \\ 0 & -1 \end{pmatrix} \quad \boldsymbol{\sigma}_2 = \begin{pmatrix} 0 & 1 \\ 1 & 0 \end{pmatrix} \quad \boldsymbol{\sigma}_3 = \begin{pmatrix} 0 & -i \\ i & 0 \end{pmatrix} \tag{9.A.2}$$

This operation is associative with addition,

$$\begin{aligned}
\mathbf{M}(\mathbf{q}_1 + \mathbf{q}_2, \mathbf{q}_3) &= \mathbf{M}(\mathbf{q}_1, \mathbf{q}_3) + \mathbf{M}(\mathbf{q}_2, \mathbf{q}_3) \\
\mathbf{M}(\mathbf{q}_1, \mathbf{q}_2 + \mathbf{q}_3) &= \mathbf{M}(\mathbf{q}_1, \mathbf{q}_2) + \mathbf{M}(\mathbf{q}_1, \mathbf{q}_3)
\end{aligned} \tag{9.A.3}$$

and associative with multiplication by a scalar,

$$\begin{aligned}
\mathbf{M}(k\mathbf{q}_1, \mathbf{q}_2) &= k\mathbf{M}(\mathbf{q}_1, \mathbf{q}_2) \\
\mathbf{M}(\mathbf{q}_1, k\mathbf{q}_2) &= k\mathbf{M}(\mathbf{q}_1, \mathbf{q}_2)
\end{aligned} \tag{9.A.4}$$

Although it is not commutative, the following relationship holds:

$$\mathbf{M}(\mathbf{q}_1, \mathbf{q}_2^\dagger) = [\mathbf{M}(\mathbf{q}_2, \mathbf{q}_1^\dagger)]^* \tag{9.A.5}$$

If $\mathbf{q}_1 \neq \mathbf{q}_2^\dagger$, the matrix $\mathbf{M}(\mathbf{q}_1, \mathbf{q}_2^\dagger)$ is complex. The Mueller matrix $\mathbf{M}(\mathbf{q}, \mathbf{q}^\dagger)$, which is real, is the Mueller matrix equivalent of the scattering matrix $\mathbf{q}$.

## References

[1] J.C. Stover, *Optical Scattering: Measurement and Analysis*, 2nd edition (SPIE Optical Engineering Press, Bellingham, WA, 1995).

[2] P. Müller-Buschbaum, J.S. Gutmann, C. Lorenz, T. Schmitt, and M. Stamm, "Decay of interface correlation in thin polymer films," Macromolecules **31**, 9265–9272 (1998).

[3] W.S. Bickel, R.R. Zito, and V. Iafelice, "Polarized Light Scattering From Metal Surfaces," J. Appl. Phys. **61**, 5392–5398 (1987).

[4] V.J. Iafelice and W.S. Bickel, "Polarized Light-Scattering Matrix Elements for Select Perfect and Perturbed Optical Surfaces," Appl. Opt. **26**, 2410–2415 (1987).

[5] G. Videen, J.-Y. Hsu, W.S. Bickel, and W.L. Wolfe, "Polarized light scattered from rough surfaces," J. Opt. Soc. Am. A **9**, 1111–1118 (1992).

[6] T.A. Germer, "Angular dependence and polarization of out-of-plane optical scattering from particulate contamination, subsurface defects, and surface microroughness," Appl. Opt. **36**, 8798–8805 (1997).

[7] T.A. Germer and C.C. Asmail, "Polarization of light scattered by microrough surfaces and subsurface defects," J. Opt. Soc. Am. A **16**, 1326–1332 (1999).

[8] F.E Nicodemus, J.C. Richmond, J.J.Hsia, I.W. Ginsberg, and T. Limperis, *Geometrical Considerations and Nomenclature for Reflectance*, NBS Monograph 160 (National Bureau of Standards, Gaithersburg, MD).

[9] C. Asmail, J. Hsia, A. Parr, and J. Hoeft, "Rayleigh scattering limits for low-level bidirectional reflectance distribution function measurements," Appl. Opt. **33**, 6084–6091 (1994).

[10] R.M.A. Azzam and N.M. Bashara, *Ellipsometry and Polarized Light* (Elsevier, Amsterdam, 1977).

[11] D.S. Flynn and C. Alexander, "Polarized surface scattering expressed in terms of a bidirectional reflectance distribution function matrix," Opt. Eng. **34**, 1646–1650 (1995).

[12] T.A. Germer and C.C. Asmail, "Goniometric optical scatter instrument for out-of-plane ellipsometry measurements," Rev. Sci. Instr. **70**, 3688–3695 (1999).

[13] SEMI ME1392, "Guide for Angle Resolved Optical Scatter Measurements on Specular or Diffuse Surfaces," (Semiconductor Equipment and Materials International, San José, CA, 2005).

[14] ASTM E2387, "Standard Practice for Goniometric Optical Scatter Measurements," (ASTM International, West Conshohocken, PA, 2005).

[15] J.W. Goodman, "Statistical Properties of Laser Speckle Patterns," in *Laser Speckle and Related Phenomena*, J.C. Dainty, Ed. (Springer-Verlag, Berlin, 1984).

[16] R.M.A. Azzam, "Photopolarimetric measurement of the Mueller matrix by Fourier analysis of a single detected signal," Opt. Lett. **2**, 148–150 (1978).

[17] D.S. Sabatke, M.R. Descour, E.L. Dereniak, W.C. Sweatt, S.A. Kemme, and G.S. Phipps, "Optimization of retardance for a complete Stokes polarimeter," Opt. Lett. **25**, 802–804 (2000).

[18] J.S. Tyo, "Design of optimal polarimeters: maximization of signal-to-noise ratio and minimization of systematic error," Appl. Opt. **41**, 619–630 (2002).

[19] A. De Martino, Y.-K. Kim, E. Garcia-Caurel, B. Laude, B. Drévillon, "Optimized Mueller polarimeter with liquid crystals," Opt. Lett. **28**, 616–618 (2003).

[20] G.E. Jellison and F.A. Modine, "Two-modulator generalized ellipsometry: theory," Appl. Opt. **36**, 8190–8198 (1997).

[21] S.O. Rice, "Reflection of Electromagnetic Waves from Slightly Rough Surfaces," Comm. Pure and Appl. Math. **4**, 351–378 (1951).

[22] D.E. Barrick, "Rough Surfaces," in *Radar Cross Section Handbook*, G.T. Ruck, ed., (Plenum, New York, 1970).

[23] T.V. Vorburger, E. Marx, and T.R. Lettieri, "Regimes of surface roughness measurable with light scattering," Appl. Opt. **32**, 3401–3408 (1993).

[24] T. Karabacak, Y.-P. Zhao, M. Stowe, B. Quayle, G.-C. Wang, and T.-M. Lu, "Large angle in-plane light scattering from rough surfaces," Appl. Opt. **39**, 4658 (2000).

[25] J.M. Elson, "Theory of light scattering from a rough surface with an inhomogeneous dielectric permittivity," Phys. Rev. B **30**, 5460–5480 (1984).

[26] J.M. Elson, "Characteristics of far-field scattering by means of surface roughness and variations in subsurface permittivity," Waves in Random Media **7**, 303–317 (1997).

[27] J.M. Elson, J.M. Bennett, and J.C. Stover, "Wavelength and angular dependence of light scattering from beryllium: comparison of theory and experiment," Appl. Opt. **32**, 3362–3376 (1993).

[28] T.A. Germer, C.C. Asmail, and B.W. Scheer, "Polarization of out-of-plane scattering from microrough silicon," Opt. Lett. **22**, 1284–1286 (1997).

[29] L. Sung, G.W. Mulholland, and T.A. Germer, "Polarized light-scattering measurements of dielectric spheres upon a silicon surface," Opt. Lett. **24**, 866–868 (1999).

[30] J.H. Kim, S.H. Ehrman, G.W. Mulholland, and T.A. Germer, "Polarized light scattering by dielectric and metallic spheres on silicon wafers," Appl. Opt. **41**, 5405–5412 (2002).

[31] T.A. Germer and C.C. Asmail, "Microroughness-blind optical scattering instrument," United States Patent #6,034,776 (2000).

[32] H.G. Tompkins, *A User's Guide to Ellipsometry* (Academic Press, New York, 1993).

[33] T.A. Germer, "Measurement of roughness of two interfaces of a dielectric film by scattering ellipsometry," Phys. Rev. Lett. **85**, 349–352 (2000).

[34] T.A. Germer, "Polarized light scattering by microroughness and small defects in dielectric layers," J. Opt. Soc. Am. A **18**, 1279–1288 (2001).

[35] J.M. Elson, "Light scattering from surfaces with a single dielectric overlayer," J. Opt. Soc. Am. **66**, 682–694 (1976).

[36] J.M. Elson, "Infrared light scattering from surfaces covered with multiple dielectric overlayers," Appl. Opt. **16**, 2872–2881 (1977).

[37] J.M. Elson, "Diffraction and diffuse scattering from dielectric multilayers," J. Opt. Soc. Am. **69**, 48–54 (1979).

[38] J.M. Elson, J.P. Rahn, and J.M. Bennett, "Light scattering from multilayer optics: comparison of theory and experiment," Appl. Opt. **19**, 669–679 (1980).

[39] J.M. Elson, "Multilayer-coated optics: guided-wave coupling and scattering by means of interface random roughness," J. Opt. Soc. Am. A **12**, 729–742 (1995).

[40] B.W. Scheer, "Development of a physical haze and microroughness standard," in *Flatness, Roughness, and Discrete Defect Characterization for Computer Disks, Wafers, and Flat Panel Displays*, J.C. Stover, Ed., Proc. SPIE **2862**, 78–95, (1996).

[41] C. Deumié, H. Giovannini, and C. Amra, "Ellipsometry of light scattering from multilayer coatings," Appl. Opt. **35**, 5600–5608 (1996).

[42] T.A. Germer, "Measurement of lithographic overlay by light scattering ellipsometry," in *Surface Scattering and Diffraction for Advanced Metrology II*, Z.-H. Gu, and A.A. Maradudin, Eds., Proc. SPIE **4780**, 72–79 (2002).

[43] T.A. Germer and M.J. Fasolka, "Characterizing surface roughness of thin films by polarized light scattering," in *Advanced Characterization Techniques for Optics, Semiconductors, and Nanotechnologies*, A. Duparré and B. Singh, Eds., Proc. SPIE **5188**, 264–275 (2003).